Journal of Solid State Chemistry 332 (2024) 124591

Contents lists available at ScienceDirect

Journal of Solid State Chemistry

journal homepage: www.elsevier.com/locate/jssc

Divalent doping of the $EuPd_3S_4$ mixed valence system

Emma A. Pappas [a,b,*], D.H. Ryan [a]

[a] Physics Department and Centre for the Physics of Materials, McGill University, 3600 University Street, Montreal, Quebec, H3A 2T8, Canada
[b] Department of Physics and Materials Research Laboratory, University of Illinois at Urbana-Champaign, 104 South Goodwin Avenue, Urbana, IL 61801, USA [1]

ARTICLE INFO

Keywords:
Europium palladium sulphide
Mixed-valency
Mössbauer spectroscopy
Divalent doping

ABSTRACT

We investigate the solubility of divalent alkaline earths calcium and strontium in $EuPd_3S_4$ where Eu^{2+} and Eu^{3+} ions are present in equal amounts on distinct sublattices. Contrary to a recent yttrium and lanthanum substitution study where complete europium replacement is possible, and there are significant changes in the europium valence, here we observe severely limited solubility ($x \lesssim 0.1$ (Ca) and $x \lesssim 0.25$ (Sr)) with a simple direct replacement of Eu^{2+} ions and no effects on the europium valence.

1. Introduction

The rare earth palladium sulphides RPd_3S_4 are remarkable in that whereas they form with the majority of the trivalent rare earths, including yttrium [1–4], when grown with europium [5] or ytterbium [4], a roughly 50:50 mix of divalent and trivalent rare earth is found. The reported 2+:3+ ratios are 54:46 in $EuPd_3S_4$ [5] and 45:55 in $YbPd_3S_4$ [4], somewhat outside the quoted uncertainties for the 50:50 that would be expected for simple charge ordering between two rare earth sites. Furthermore, there is a significant size difference between the valence states in both Eu and Yb, and an ordered arrangement might be expected to result in a distortion of the crystal cell. Such a distortion could be accommodated by lowering the crystal symmetry from $Pm\bar{3}n$ (space group #223), reported for RPd_3S_4 with the trivalent rare earths, to $Pm\bar{3}$ (#200). This allows for the displacement of the palladium and sulphur atoms from their special positions in the $Pm\bar{3}n$ structure and splits the original 2*a* rare earth site into 1*a* at (000) and 1*b* at $(\frac{1}{2}\frac{1}{2}\frac{1}{2})$. Recent single crystal X-ray diffraction measurements have confirmed that this distortion occurs below 340 K in $EuPd_3S_4$ and that it leads to volume difference between the two europium sites, the 1*b* being about 10% larger [6]. It is likely that this distortion was missed in earlier work because powder samples were used, and the intensity changes in the powder diffraction pattern are extremely small. The characteristic 100 peak (only allowed for the $Pm\bar{3}$ space group) is ~0.1% of the strongest 211 reflection.

We recently investigated the stability of the Eu^{2+}:Eu^{3+} ratio in $EuPd_3S_4$ by replacing the europium with unambiguously trivalent yttrium and lanthanum [7]. We found that yttrium substitution promoted $Eu^{3+} \rightarrow Eu^{2+}$ conversion whereas lanthanum had essentially no effect until about half of the europium had been replaced, after which it promoted $Eu^{2+} \rightarrow Eu^{3+}$ conversion. The differing impacts on the europium valence distribution was attributed to the system preferring to maintain a constant average rare earth size.

Here we investigate the impacts of divalent substitutions for europium. The size of Ca^{2+} lies between those of Eu^{3+} and Eu^{2+}, while Sr^{2+} is closer in size to the larger Eu^{2+} ion [8]. Strontium might be expected to replace the 50% Eu^{2+} in $EuPd_3S_4$ without causing significant volumetric or valence issues, but calcium will cause problems in whichever site it substitutes. Following the reported effects of Y and La substitution [7], we also anticipate changes in the Eu^{2+}:Eu^{3+} ratio here as Ca/Sr are added. ^{151}Eu Mössbauer provides direct access to the Eu^{2+}:Eu^{3+} valence ratio while X-ray powder diffraction is used to follow changes in the lattice parameter and to both identify and quantify impurities. There is sufficient scattering contrast between europium and the two elements (Ca and Sr) used to replace it that reliable chemical compositions could be determined from powder diffraction patterns. Compositions were also checked for selected samples using energy dispersive spectroscopy (EDS), however this proved less accurate, possibly due to the very different atomic numbers of the key elements, so these results are only presented in the appendix.

In contrast to our earlier yttrium and lanthanum substitution work where we found that $(Y,La)_xEu_{1-x}Pd_3S_4$ exists for all x [7], there is quite limited solubility for the divalent alkaline earths and $(Ca,Sr)_xEu_{1-x}Pd_3S_4$ only exist for $x \lesssim 0.1$ (Ca) and $x \lesssim 0.25$ (Sr). Fur-

* Corresponding author at: Department of Physics and Materials Research Laboratory, University of Illinois at Urbana-Champaign, 104 South Goodwin Avenue, Urbana, IL 61801, USA.
E-mail address: epappas3@illinois.edu (E.A. Pappas).
[1] Current address.

https://doi.org/10.1016/j.jssc.2024.124591
Received 29 December 2023; Received in revised form 26 January 2024; Accepted 1 February 2024
Available online 9 February 2024

thermore, we find that both calcium and strontium appear to simply replace Eu^{2+} without promoting any valence changes, despite the significant differences between the sizes of the Ca^{2+} and Sr^{2+} ions.

2. Experimental methods

Polycrystalline samples of $EuPd_3S_4$ and $(Ca,Sr)_xEu_{1-x}Pd_3S_4$ were prepared from stoichiometric mixtures of EuS (99.9% – American Elements) CaS (99.9%), SrS (99.9%), Pd (99.95%) and S (99.5%), all from Alfa-Aesar. The powders were mixed and then pressed to form a dense pellet. The pellet was loaded into an alumina crucible and sealed under a partial pressure of helium in a fused silica tube. The sample was heated to 650 °C over three hours, held for an hour and then taken to 900 °C over a further three hours. After 75 hours at 900 °C the sample was furnace cooled and removed once it reached ambient temperature. Incomplete reaction was observed with the impurity levels increasing with increasing Ca/Sr substitution. Samples were ground, pressed and re-annealed at 900 °C for a further 75 hours but only minor changes were achieved. For the calcium-containing samples we observed devitrification of the interior surface of the fused silica tubes. This damage became more severe with increasing calcium content leading, during our attempt to synthesize the pure $CaPd_3S_4$ compound, to a complete failure of the tube. The primary impurity found was PdS, with SrS being detected in increasing amounts as the level of strontium doping was increased. Unreacted CaS was not seen, either because the excess calcium had reacted with the fused silica tube, or because it is a much weaker X-ray scatterer than the other components. See below for more details.

Ambient-temperature X-ray diffraction measurements were made on a Bruker Phaser-II diffractometer equipped with a Linxeye XE-T linear strip detector using a Cu-K_α source. Full Rietveld refinement of the diffraction patterns was carried out using the GSAS-II package [9]. In light of the extremely small differences between the diffraction patterns from the $Pm\bar{3}n$ and $Pm\bar{3}$ structures, all refinements presented here assume that the samples retained the $NaPt_3O_4$ ($Pm\bar{3}n$ #223) structure with the (Eu,Ca,Sr) on the 2*a* site, Pd on the 6*d* site and S on the 8*e* site. Refinement using the $Pm\bar{3}$ structure and permitting selective substitution on the 1*a* and 1*b* sites did not materially change the results, but did lead to larger uncertainties on the derived compositions.

^{151}Eu Mössbauer spectroscopy measurements were carried out using a 4 GBq $^{151}SmF_3$ source, driven in sinusoidal mode. The drive motion was calibrated using a standard ^{57}Co<u>Rh</u>/α-Fe foil. Isomer shifts are quoted relative to EuF_3 at ambient temperature. The 21.6 keV gamma rays were recorded using a thin NaI scintillation detector. Samples were cooled in a vibration-isolated closed-cycle helium refrigerator with the sample in a helium exchange gas. As no quadrupole or magnetic effects were observed, the spectra were simply fitted to a sum of two Lorentzian lines, one for each valence state of the europium ions.

3. Results and discussion

3.1. Analysis of X-ray diffraction data for $(Ca,Sr)_xEu_{1-x}Pd_3S_4$

Powder X-ray diffraction measurements were used to determine the chemical compositions of samples of $(Ca,Sr)_xEu_{1-x}Pd_3S_4$. Figs. 1 and 2 show fitted data for representative samples doped with calcium and strontium respectively. These examples were chosen as they exhibit all of the impurity phases encountered. We note that in samples with a nominal strontium content below 0.25, no SrS impurity was detected. The $NaPt_3O_4$ structure ($Pm\bar{3}n$ #223) was used for the refinement of all data presented in this report. For the $(Ca,Sr)_xEu_{1-x}Pd_3S_4$ phase, refined parameters include the microstrain, lattice parameter, fractional occupation of the dopant on the 2*a* site, and thermal parameters of all atoms. The thermal parameters for calcium and strontium were constrained to the value for europium in order to obtain stable fits and avoid unphysical values. The weight fraction of the relevant impurities and 6 to 8 background terms were also used in the refinements. When

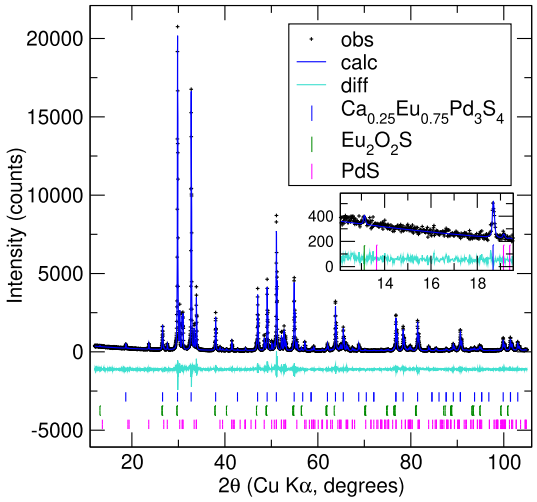

Fig. 1. Cu-K_α X-ray diffraction pattern for sample with nominal composition $Ca_{0.25}Eu_{0.75}Pd_3S_4$. Rietveld refinement (blue solid line) overlaps the data (black crosses) with residuals (teal solid line) underneath. Tick marks at the bottom show the positions of the Bragg peaks for the main phase $Ca_{0.25}Eu_{0.75}Pd_3S_4$ (blue), and for the small impurity phases Eu_2O_2S (green) and PdS (pink). The inset is a zoomed-in view of the low-angle data and shows the very small peak close to 13° due to 3.86(9) wt.% of Eu_2O_2S.

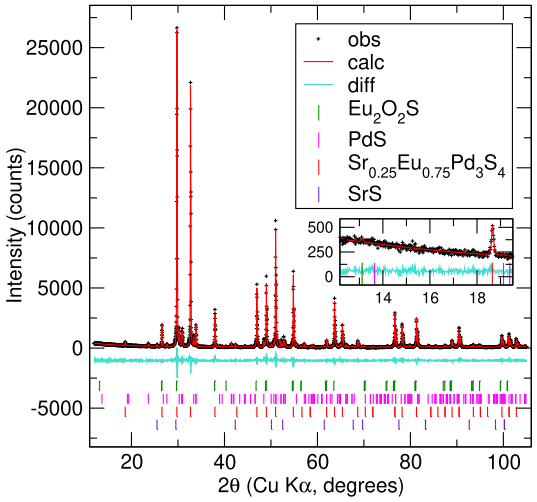

Fig. 2. Cu-K_α X-ray diffraction pattern for sample with nominal composition $Sr_{0.25}Eu_{0.75}Pd_3S_4$. Rietveld refinement (red solid line) overlaps the data (black crosses) with residuals (teal solid line) underneath. Tick marks at the bottom show the positions of the Bragg peaks for the main phase $Sr_{0.25}Eu_{0.75}Pd_3S_4$ (red), and for the small impurity phases Eu_2O_2S (green), PdS (pink), and SrS (purple). The inset is a zoomed-in view of the low-angle data and shows the very small peak close to 13° due to 1.99(9) wt.% of Eu_2O_2S.

the PdS and SrS impurities were present in significant amounts, their lattice parameters were refined.

Upon careful examination of the XRD patterns, highly doped samples displayed visible Eu_2O_2S diffraction peaks from 13° to 80°. The major diffraction peaks around 26.5°, 29.7°, 37.8°, and 46.8° (corresponding to the 100 and 002, 101 and 10$\bar{1}$, 102 and 10$\bar{2}$, and 110 characteristic peaks) were used to identify this impurity. [10,11] These major diffraction peaks overlap with peaks of the main phase and PdS impurity, making the small Eu_2O_2S impurity less noticeable in some samples. Nevertheless, visual comparison of residuals before and after the inclusion of the Eu_2O_2S phase in the refinements confirmed its presence. Small amounts of Eu_2O_2S were detected in all samples, possibly due to oxidation of the products or reactants (see Tables 1 and 2).

Table 1
Measured compositions, ambient-temperature lattice parameters, Eu^{2+} fractions determined from ^{151}Eu Mössbauer spectroscopy at 5K, and weight percent impurities for the $Ca_xEu_{1-x}Pd_3S_4$ compound series. The "A" in the final column indicates the data were taken from a sample that had been re-ground, pressed, and annealed a second time.

Composition		a (Å)	Total	Eu^{2+} fraction in	PdS	Eu_2O_2S	
Nominal	Measured		Eu^{2+} (%)	$Ca_xEu_{1-x}Pd_3S_4$ (%)	(wt.%)	(wt.%)	
0.00	0.00	6.67753(4)	53.8(4)	55.7(4)	2.31(7)	1.07(9)	–
0.00	0.00	6.67738(5)	53.7(6)	55.2(6)	1.02(6)	0.80(8)	A
0.10	0.017(8)	6.67521(5)	50.1(6)	55.6(6)	6.23(9)	3.01(9)	–
0.10	0.002(8)	6.67542(5)	52.7(6)	57.2(6)	9.97(10)	2.32(9)	A
0.175	0.021(10)	6.67305(7)	47.6(6)	54.7(7)	21.36(15)	3.36(9)	–
0.175	0.040(9)	6.67357(10)	50.3(6)	54.2(6)	10.10(11)	2.06(9)	A
0.25	N/A	N/A	45.2(4)	N/A	N/A	N/A	–
0.25	0.073(10)	6.67196(7)	44.3(6)	52.3(8)	22.27(14)	3.86(9)	A
0.35	0.132(14)	6.66784(8)	36.9(6)	53(1)	38.15(20)	6.57(10)	–
0.35	0.112(11)	6.66833(6)	40.2(5)	53.6(7)	30.22(16)	5.91(9)	A

Table 2
Measured compositions, ambient-temperature lattice parameters, Eu^{2+} fractions determined from ^{151}Eu Mössbauer spectroscopy at 5K, and weight percent impurities for the $Sr_xEu_{1-x}Pd_3S_4$ compound series. The "A" in the final column indicates the data were taken from a sample that had been re-ground, pressed, and annealed a second time.

Composition		a (Å)	Total	Eu^{2+} fraction in	PdS	Eu_2O_2S	SrS	
Nominal	Measured		Eu^{2+} (%)	$Sr_xEu_{1-x}Pd_3S_4$ (%)	(wt.%)	(wt.%)	(wt.%)	
0.00	0.00	6.67753(4)	53.8(4)	55.7(4)	2.31(7)	1.07(9)	0.00	–
0.00	0.00	6.67738(5)	53.7(6)	55.2(6)	1.02(6)	0.80(8)	0.00	A
0.10	0.041(16)	6.67866(8)	N/A	N/A	3.19(7)	1.30(9)	0.00	–
0.10	0.039(16)	6.67855(9)	51.7(5)	53.3(5)	1.71(6)	0.87(9)	0.00	A
0.15	0.109(14)	6.68003(5)	45.7(6)	47.9(7)	3.20(6)	1.26(8)	0.00	–
0.15	0.089(15)	6.67956(5)	46.9(6)	49.3(7)	2.75(6)	1.41(8)	0.00	A
0.20	0.167(16)	6.68061(6)	40.8(7)	44.4(8)	6.74(8)	2.09(9)	0.00	–
0.20	0.152(16)	6.68044(6)	43.5(7)	45.7(7)	4.83(7)	1.23(9)	0.00	A
0.25	N/A	N/A	37.8(8)	N/A	N/A	N/A	N/A	–
0.25	0.173(16)	6.68178(5)	38.2(8)	41.6(9)	10.65(9)	1.99(9)	1.23(5)	A
0.35	0.188(23)	6.68170(5)	34.3(6)	43.0(8)	22.42(16)	4.36(11)	6.15(9)	–
0.35	0.211(23)	6.68218(5)	31.4(6)	41(1)	25.15(16)	4.88(12)	5.88(9)	A
0.50	0.204(35)	6.68151(9)	31.0(7)	39(1)	39.89(23)	3.20(12)	9.08(12)	–
0.50	0.247(34)	6.68160(11)	32.7(6)	42(1)	36.33(22)	3.78(12)	6.97(10)	A

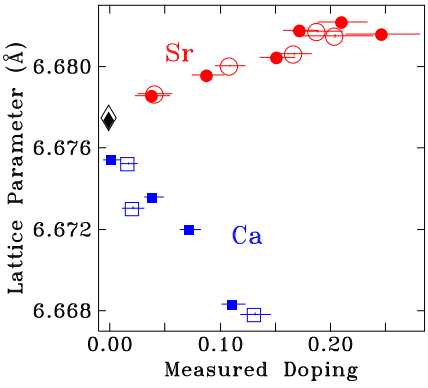

Fig. 3. Lattice parameters for $(Ca,Sr)_xEu_{1-x}Pd_3S_4$ plotted vs. the fitted doping level. Doping with strontium (red circles) leads to a modest increase in lattice parameter, while the much smaller calcium ion (blue squares) leads to a marked contraction. Open symbols show values taken from samples as made. Solid symbols show values taken from re-annealed samples. The solid black diamond shows the value for the parent compound $EuPd_3S_4$. Horizontal bars show the uncertainties derived from the fits to the X-ray diffraction data. Uncertainties in the lattice parameters are too small to show.

The fractional occupation of calcium and strontium and the lattice parameters of the $(Ca,Sr)_xEu_{1-x}Pd_3S_4$ compounds are presented in Tables 1 and 2. As can be seen in Fig. 3, strontium substitution leads to a modest expansion of the lattice, while calcium leads to a more rapid contraction, suggesting that Eu^{2+} ions are being replaced by the dopants. Fig. 4 shows the limited solubility of calcium and strontium in $EuPd_3S_4$, which explains the presence of PdS and SrS impurities in the XRD data. The solubility of the divalent ions is discussed in more detail below.

Refinements using the lower symmetry $Pm\bar{3}$ structure [6] with selective substitution on the 1*a* and 1*b* sites were attempted but were excluded for lack of evidence for this structure in our data. As noted earlier, only the presence of a weak 100 peak located near $2\theta = 13°$ distinguishes the $Pm\bar{3}$ structure from the higher symmetry $Pm\bar{3}n$ structure. Unfortunately, this diffraction peak overlaps with the characteristic 001 peak of the Eu_2O_2S impurity present in the data (see the insets of Figs. 1 and 2). With a weight fraction varying between 0.80(8) wt.% and 6.57(10) wt.%, even this small Eu_2O_2S impurity is sufficient to hide any potential indication of the $Pm\bar{3}$ structure.

3.2. *Solubility limits for Ca and Sr in* $EuPd_3S_4$

It is clear from Fig. 4 that the Ca/Sr content of the $(Ca,Sr)_xEu_{1-x}Pd_3S_4$ phase is always lower than that of the initial mixture, with the calcium content significantly lower than the corresponding strontium sample. The compositions of the Sr-doped samples show evidence of saturation, suggesting a limiting composition of $x \sim 0.25$ in $Sr_xEu_{1-x}Pd_3S_4$. We were unable to exceed $x \sim 0.1$ in $Ca_xEu_{1-x}Pd_3S_4$. Since we start with an (intended) stoichiometric mixture, incomplete substitution leaves excess palladium, sulphur and (Ca,Sr)S. While we did find some evidence of unreacted SrS, CaS was not found, either because it was too

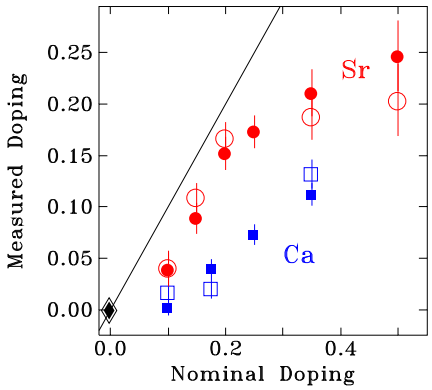

Fig. 4. Comparison of the fitted (Ca,Sr) compositions derived from analysis of the X-ray diffraction patterns, with the nominal values derived from the initial composition of the sample pellet. Values for strontium are shown as red circles, values for calcium are shown as blue squares. Open symbols show values taken from samples as made. Solid symbols show values taken from re-annealed samples. Whereas the doping level clearly increases as more (Ca,Sr) is included in the initial mix, in both cases the fitted composition shows less doping than expected. This deviation is especially acute for calcium. For strontium doping we see evidence of saturation, suggesting a solubility limit of about 0.25.

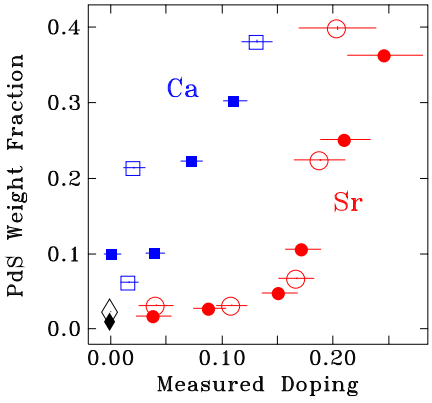

Fig. 5. Fitted weight fraction of the PdS impurity plotted vs. the fitted doping level for $(Ca,Sr)_xEu_{1-x}Pd_3S_4$. Values for strontium are shown as red circles, values for calcium are shown as blue squares. Open symbols show values taken from samples as made. Solid symbols show values taken from re-annealed samples. For $Sr_xEu_{1-x}Pd_3S_4$ there is a rapid growth for $x \geq 0.15$ as we approach the solubility limit for strontium in $EuPd_3S_4$. The more limited solubility for calcium is reflected in the much higher impurity levels even at quite low doping levels.

weak a scatterer or because the excess calcium reacted with the silica tube. The clearest impurity phase was the tetragonal PdS which gave a strong diffraction signature, and as Fig. 5 shows, the growth in the PdS fraction tracks the growing gap between measured and nominal doping in Fig. 4. For Ca-doping the PdS fraction simply grows steadily, as the measured doping is consistently about $\frac{1}{3}$ of the nominal value. By contrast, for Sr doping we see very little PdS until we reach a nominal level of $x \sim 0.15$, after which the PdS fraction grows rapidly as we approach saturation.

3.3. *Valence effects of Ca and Sr doping of* $EuPd_3S_4$

^{151}Eu Mössbauer spectra of $Ca_xEu_{1-x}Pd_3S_4$ (Fig. 6) and $Sr_xEu_{1-x}Pd_3S_4$ (Fig. 7) were taken at 5 K to minimise the effects of differing f−factors for the Eu^{2+} and Eu^{3+} ions [7]. In both cases we see a clear reduction in the Eu^{2+} peak near −10 mm/s with increasing doping. The effect is larger in the Sr-doped series primarily because we achieve greater doping levels for Sr compared with Ca. From the X-ray diffraction analysis, we know that we do not attain complete doping at any composition, so we always have excess, unreacted Ca or Sr in the samples with $(Ca,Sr)_xEu_{1-x}Pd_3S_4$ and Eu_2O_2S being the only Eu-containing phases present. The presence of Eu_2O_2S means that the Eu^{2+}:Eu^{3+} ratio determined from the ^{151}Eu Mössbauer spectra does not directly reflect the valence ratio in the $(Ca,Sr)_xEu_{1-x}Pd_3S_4$ phase

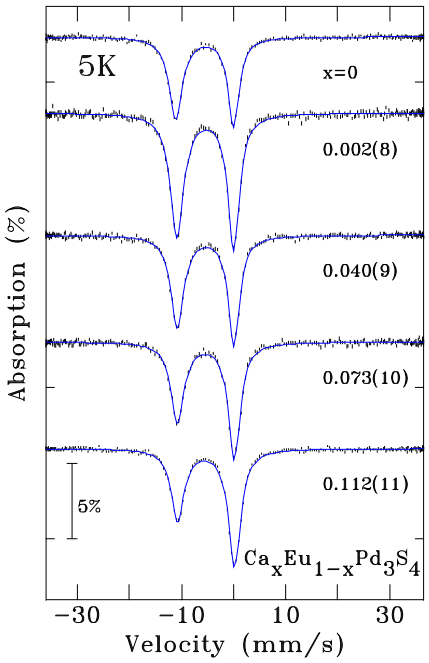

Fig. 6. ^{151}Eu Mössbauer spectra of $Ca_xEu_{1-x}Pd_3S_4$ at 5 K showing the gradual reduction of the Eu^{2+} component (the line at ∼ −10 mm/s) as the level of calcium substitution increases. The values for the doping level, x, are taken from analysis of the X-ray diffraction data. These spectra were measured on re-annealed samples.

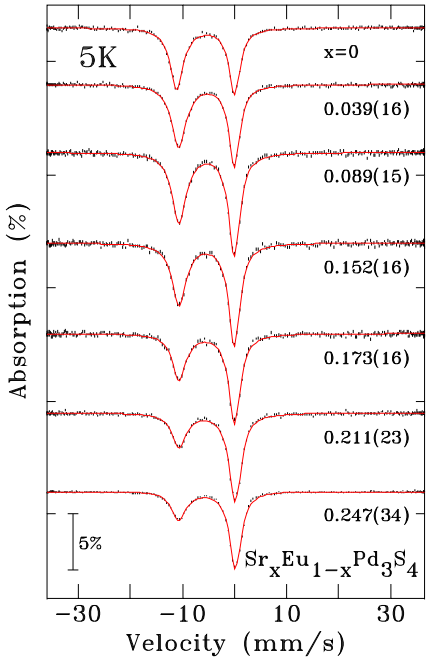

Fig. 7. ^{151}Eu Mössbauer spectra of $Sr_xEu_{1-x}Pd_3S_4$ at 5 K showing the marked reduction of the Eu^{2+} component (the line at ∼ −10 mm/s) as the level of strontium substitution increases. The values for the doping level, x, are taken from analysis of the X-ray diffraction data. These spectra were measured on re-annealed samples.

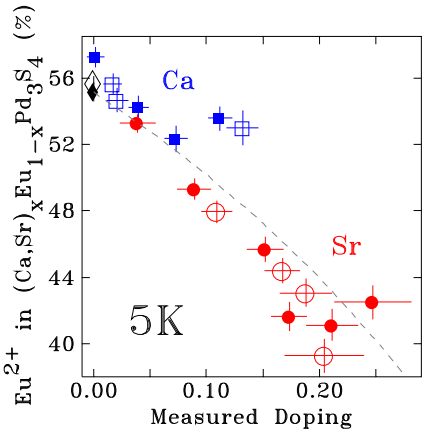

Fig. 8. Eu^{2+} fraction in $(Ca,Sr)_xEu_{1-x}Pd_3S_4$ derived from analysis of the ^{151}Eu Mössbauer spectra at 5K. The data shows a clear decrease in Eu^{2+} content as calcium or strontium is substituted for europium. The dashed line shows a fit that indicates that for each Ca/Sr atom added, one Eu^{2+} ion is lost, suggesting that the divalent ions simply replace the Eu^{2+} ions without leading to any changes in the valence of the remaining europium ions.

we are studying. However, we can correct the valence ratio to reflect that of the phase of interest by using the measured weight fraction of Eu_2O_2S determined by our analysis of the X-ray diffraction data (see Tables 1 and 2). This europium distribution along with the fact that the europium in Eu_2O_2S is fully trivalent [11] allows us to calculate the portion of Eu^{3+} signal coming from Eu_2O_2S and thus determine the Eu^{2+}:Eu^{3+} ratio in $(Ca,Sr)_xEu_{1-x}Pd_3S_4$. The results of this analysis are shown in Tables 1 and 2.

Fig. 8 shows that both Ca and Sr replacements lead to a reduction in the Eu^{2+} component in $(Ca,Sr)_xEu_{1-x}Pd_3S_4$ that appears to scale approximately linearly with their measured doping level. A more detailed analysis (dashed line in Fig. 8) shows that for every divalent dopant atom added to the system, one Eu^{2+} ion is lost, so that neither dopant leads to any apparent $Eu^{2+} \rightarrow Eu^{3+}$ conversion. Given the very similar size of the Sr^{2+} and Eu^{2+} ions, it is not too surprising to find a simple one-to-one substitution of the divalent ions. On the other hand, one could expect the smaller Ca^{2+} ion to cause some $Eu^{2+} \rightarrow Eu^{3+}$ conversion, which is not observed here. Indeed, our most calcium rich points actually lie *above* the calculated line, *i.e.* implying a possible, but unlikely, $Eu^{3+} \rightarrow Eu^{2+}$ conversion.

The one-to-one substitution of the divalent ions goes some way to accounting for the limited calcium solubility in $EuPd_3S_4$, which likely results from increasing strain as the smaller Ca^{2+} replaces the larger Eu^{2+} ions. The rapid decrease in lattice parameter apparent in Fig. 3 is a clear consequence of substituting the smaller Ca^{2+} ion. While $Eu^{3+} \rightarrow Eu^{2+}$ conversion could, in principle, compensate for the Ca-induced contraction, this would likely create additional strains on the Eu^{3+} sublattice (assuming that the ordered $Pm\bar{3}$ is retained) suppressing any such conversion.

The size mismatch problem should be largely absent in the case of Sr^{2+}/Eu^{2+} exchange, and this is reflected in the much slower ($< \frac{1}{3}$) rate of change in lattice parameter with doping level. However, it is apparent that some other factor eventually limits the strontium solubility to $\lesssim$0.25. Strain would not appear to be a likely candidate as the maximum lattice expansion observed with strontium substitution is less than half of the contraction achieved with calcium.

The effects of substitution with both divalent alkaline earth ions thus support conservation of the total valence electron counts. However, the calcium substitution gives a similar behaviour as was previously observed for low La^{3+} substitution, where lanthanum only started to promote $Eu^{2+} \rightarrow Eu^{3+}$ conversion after having replaced about half of the europium [7]. Given that the sizes of the calcium and lanthanum ions both lie between those of the trivalent and divalent europium, it is possible that a large substitution is necessary to produce any effect on the valence distribution of the europium ions, which has proven impossible with calcium. So the limited solubility of Ca and Sr in $EuPd_3S_4$ does not allow the exclusion of a tendency of the system to maintain a constant rare earth size, as was found with trivalent rare earth substitution.

4. Conclusions

In contrast to the effects of trivalent (Y, La) substitutions for europium in $EuPd_3S_4$, where significant changes in the europium valence balance was observed [7], divalent substitution using Ca or Sr does not appear to promote any valence changes, with the Ca^{2+}/Sr^{2+} ions simply replacing Eu^{2+} ions. Furthermore, while $(Y,La)_xEu_{1-x}Pd_3S_4$ exists for all x [7], there is quite limited solubility for the divalent alkaline earths and $(Ca,Sr)_xEu_{1-x}Pd_3S_4$ only exist for $x \lesssim 0.1$ (Ca) and $x \lesssim 0.25$ (Sr). Whereas strains due to the size mismatch between Eu^{2+} and Ca^{2+} likely play a significant role limiting the calcium solubility, it is unclear what limits the strontium solubility to $x \lesssim 0.25$, about half of what might be achieved by replacing all of the Eu^{2+} ions in $EuPd_3S_4$.

CRediT authorship contribution statement

Emma A. Pappas: Writing – review & editing, Writing – original draft, Visualization, Validation, Project administration, Methodology, Investigation, Formal analysis, Data curation, Conceptualization. **D.H. Ryan:** Writing – review & editing, Writing – original draft, Supervision, Software, Resources, Methodology, Funding acquisition, Conceptualization.

Declaration of competing interest

The authors declare that they have no known competing financial interests or personal relationships that could have appeared to influence the work reported in this paper.

Data availability

The data that support the findings of this study are available from the corresponding author upon reasonable request.

Acknowledgements

Financial support for this work was provided by Fonds Québécois de la Recherche sur la Nature et les Technologies, and the Natural Sciences and Engineering Research Council (NSERC) Canada. The assistance of Sidney Omelon and Tian Zhao with the X-ray diffraction work is gratefully acknowledged. The authors acknowledge the use of facilities and instrumentation at the Materials Research Laboratory Central Research Facilities, University of Illinois, for the energy dispersive spectroscopy work.

Appendix A. EDS results

The chemical composition of some re-annealed polycrystalline samples in the $(Ca,Sr)_xEu_{1-x}Pd_3S_4$ compound series was analyzed using a scanning electron microscope (SEM) with energy dispersive spectroscopy (EDS). Measurements were made on a ThermoFisher Axia ChemiSEM with an accelerating voltage of 20kV and a spot size of 5. Impurities were avoided by collecting quantitative elemental mappings on what appeared to be single grains of uniform composition. The chemical compositions averaged over multiple 30-second measurements are presented in Table 3. A minimum of three regions was considered for the samples with a nominal dopant content of 0.35. The sparsity of impurities in samples with lower doping allowed for more than ten regions to be considered in the averagings. The EDS results confirm the presence

Table 3
SEM-EDS data for some re-annealed samples in the $(Ca,Sr)_xEu_{1-x}Pd_3S_4$ compound series. The reported elemental atomic fractions are averaged over multiple regions and accompanied by their standard errors. The scaled dopant contents are included for easy comparison with the nominal contents.

Dopant				Eu	Pd	S
	Nominal	Scaled	(at. %)	(at. %)	(at. %)	(at. %)
Ca	0.35	0.150(5)	2.07(7)	11.7(1)	38.1(1)	48.1(1)
Ca	0.175	0.046(3)	0.62(3)	12.8(2)	38.5(2)	48.1(1)
-	0	N/A	N/A	13.6(2)	38.43(9)	47.9(1)
Sr	0.15	0.171(4)	2.61(5)	12.6(2)	37.59(9)	47.1(1)
Sr	0.25	0.21(1)	3.1(2)	11.3(4)	37.9(3)	47.7(1)
Sr	0.35	0.26(2)	4.1(2)	11.4(4)	37.1(3)	47.3(2)

of dopants in the samples, but the elemental atomic percentages do not seem accurate as they suggest non-stoichiometric ratios of europium, palladium, and sulphur in the parent compound $EuPd_3S_4$. In most samples, the europium, palladium, calcium, and strontium contents seem to be overestimated, while the sulphur content seems to be underestimated. SEM-EDS may have been less accurate in this case due to the presence of many elements with very different densities and characteristic energies.

References

[1] D.A. Keszler, J.A. Ibers, M.H. Mueller, Preparation, characterization, and physical properties of the series MPd3S4 (M = rare earth), J. Chem. Soc., Dalton Trans. (1985) 2369–2373.
[2] M. Wakeshima, T. Fujino, N. Sato, K. Yamada, H. Masuda, Crystal structure and electrical conductivity of palladium sulfide bronzes MP3S4 (M = La, Nd, and Eu), J. Solid State Chem. 129 (1997) 1–6.
[3] M. Wakeshima, Y. Hinatsu, Magnetic properties of RPd3S4 (R = Ce, Gd), J. Solid State Chem. 146 (1999) 226–229.
[4] P. Bonville, C. Godart, E. Alleno, F. Takahashi, E. Matsuoka, M. Ishikawa, Heterogeneous mixed valence in YbPd3S4: evidence from 170Yb Mossbauer and X-ray LIII-edge absorption measurements, J. Phys. Condens. Matter 15 (2003) L263–L269.
[5] M. Wakeshima, Y. Doi, Y. Hinatsu, N. Masaki, Mössbauer effects and magnetic properties of mixed valent europium sulfide, EuPd3S4, J. Solid State Chem. 157 (2001) 117–122.
[6] T. Berry, V.C. Morano, T. Halloran, X. Zhang, T.J. Slade, A. Sapkota, S.L. Budko, W. Xie, D.H. Ryan, Z. Xu, Y. Zhao, J.W. Lynn, T. Fennell, P.C. Canfield, C.L. Broholm, T.M. McQueen, Formation of a simple cubic antiferromagnet through charge ordering in a double Dirac material, arXiv:2303.02218, 2023.
[7] D.H. Ryan, S.L. Bud'ko, B. Kuthanazhi, P.C. Canfield, Valence and magnetism in $EuPd_3S_4$ and $(Y,La)_xEu_{1-x}Pd_3S_4$, Phys. Rev. B 107 (2023) 014402.
[8] R.D. Shannon, Revised effective ionic radii and systematic studies of interatomic distances in halides and chalcogenides, Acta Crystallogr. A 32 (1976) 751–767.
[9] B.H. Toby, R.B. Von Dreele, GSAS-II: the genesis of a modern open-source all purpose crystallography software package, J. Appl. Crystallogr. 46 (2013) 544–549.
[10] M. Leskelä, L. Niinistö, Solid solutions in the rare-earth oxysulfide series, J. Solid State Chem. 19 (1976) 245–250.
[11] V. Biondo, P. Sarvezuk, F. Ivashita, K. Silva, A. Paesano, O. Isnard, Geometric magnetic frustration in RE_2O_2S oxysulfides (RE = Sm, Eu and Gd), Mater. Res. Bull. 54 (2014) 41–47.